S1.1 Materials

Active Pharmaceutical Ingredient: The specific dopamine transporter inhibitor, GBR-12935 dihydrochloride, was purchased from MedChemExpress (MCE) (Monmouth Junction, NJ, USA). Hydrogel Components: Konjac glucomannan (KGM) (Viscosity >1500 mPa·s, Cat. No. S30903) was obtained from Shanghai Yuanye Bio-Technology Co., Ltd. (Shanghai, China). Chitosan (CS, Viscosity >200 mPa • s, Cat. No. HWG62417) was supplied by Beijing Hwrk Chemical Co., Ltd. (Beijing, China). The oxidation agents and quenchers, including Sodium periodate (NaIO4) (Cat. No. S104093) and Ethylene glycol (Cat. No. E119700), were purchased from Shanghai Aladdin Biochemical Technology Co., Ltd. (Shanghai, China). Antibodies for Immunofluorescence: For synaptic morphology analysis, the following primary antibodies were used: mouse anti-CtBP2 IgG1 (Cat. No. 612044) from BD Transduction Laboratories (Franklin Lakes, NJ, USA) and mouse anti-GluR2 monoclonal antibody (Clone 6C4, Cat. No. 32-0300) from Invitrogen (Thermo Fisher Scientific, Waltham, MA, USA). All other reagents and solvents were of analytical grade and used as received without further purification.

S1.2 Structural Analysis

The chemical structures of KGM and synthesized OKGM were analyzed using proton nuclear magnetic resonance (^{1}H-NMR) spectroscopy. Samples were dissolved in deuterium oxide (D_2O) at a concentration of 10 mg mL^{-1}. The spectra were recorded on a (Bruker AVANCE III 500 MHz) spectrometer at 25 ℃. To verify the crosslinking mechanism, Fourier transform infrared (FTIR) spectra of the freeze-dried hydrogel samples were acquired using a (Nicolet iS50) spectrometer. The samples were mixed with KBr powder and pressed into pellets, and scanned over the wavenumber range of 500 - 4000 cm^{-1}.

S1.3 Morphology Characterization

The internal microstructure of the hydrogels was visualized using Scanning Electron Microscopy (SEM). Hydrogel samples were fully swollen, frozen at -20 ℃, and lyophilized. The dried samples were cross-sectioned, sputter-coated with a thin layer of gold to enhance conductivity, and imaged using a scanning electron microscope (JEOL JSM-7000F) at an accelerating voltage of 5.0 kV.

S1.4 Cell Culture and Hydrogel Extract Preparation

L929 mouse fibroblasts and BEAS-2B human bronchial epithelial cells were cultured in RPMI-1640 and DMEM medium, respectively, supplemented with 10% fetal bovine serum (FBS) and 1% penicillin-streptomycin at 37 ℃ in a 5% CO_2 atmosphere. To prepare the hydrogel extracts, sterilized hydrogels (1:1 and 1:2 ratios) were immersed in the complete culture medium at a distinct extraction ratio (0.1 g mL^{-1}) and incubated at 37 ℃ for 24 h. The supernatants were collected and filtered through a 0.22 μm membrane to serve as the conditioned medium for subsequent assays.

S1.5 Cell Viability Assessment

The quantitative evaluation of cytotoxicity was performed using the Cell Counting Kit-8 (CCK-8) purchased from Beyotime Biotechnology (Shanghai, China). Both BEAS-2B epithelial cells and L929 fibroblasts were seeded into 96-well plates (5×10^3 cells/well) and allowed to adhere overnight. The culture medium was then replaced with 100 μL of the hydrogel extracts (prepared as described above). After incubation for 24, 48, and 72 h, the supernatant was removed, and 100 μL of fresh medium containing 10% CCK-8 working solution was added to each well. The plates were incubated at 37 ℃ for 1 h until the color turned orange. Finally, the optical density (OD) values were measured at 450 nm using a microplate reader. The cell viability was expressed as the percentage of absorbance relative to the control group.

S1.6 Live/Dead Staining Evaluation

Cell viability was visualized using a Calcein AM/PI Live/Dead Viability Assay Kit (Beyotime Biotechnology, Shanghai, China). BEAS-2B cells were seeded at a density of 3×10^4 cells mL^{-1} and cultured with the hydrogel extracts for 24 h and 48 h. At each time point, the cells were washed with PBS and incubated with the staining working solution (containing Calcein AM and Propidium Iodide) for 15 min at 37 °C in the dark, strictly following the manufacturer's instructions. The stained cells were subsequently imaged using a TS2R-LS inverted fluorescence microscope (Nikon, Japan) to identify live (green fluorescence) and dead (red fluorescence) cells.

S1.7 Auditory Brainstem Response (ABR) Measurement

Cochlear function was assessed by measuring ABR thresholds on Day 7 post-noise exposure. Mice were anesthetized, and subdermal needle electrodes were inserted at the vertex (active), mastoid (reference), and hind leg (ground). Acoustic stimuli consisting of tone bursts (4, 8, 16, 24, and 32 kHz) were generated using a TDT(RZ6, Tucker-Davis Tech., Alachua, FL, USA). The sound intensity was decreased in 5 dB steps from 90 dB SPL down to the visual detection threshold of the ABR waveforms.

S1.8 Immunofluorescence Staining

Following the final ABR assessment, the mice were euthanized, and the cochleae were rapidly harvested. The tissues were fixed in 4% paraformaldehyde (PFA) overnight at 4 ℃. To facilitate micro-dissection, the samples were decalcified in 10% EDTA for 1-2 days and rinsed with PBS. The organ of Corti was carefully isolated, and the basilar membrane was segmented into apical, middle, and basal turns. For immunolabeling, the dissected tissues were permeabilized and blocked simultaneously using a solution containing 0.3% Triton X-100 and 10% goat serum for 1 h at room temperature. Subsequently, the specimens were incubated overnight at 4 ℃ with primary antibodies targeting hair cells and synaptic structures: mouse anti-CtBP2 (1:200, BD Transduction Laboratories) and rabbit anti-Myosin-VIIa (1:300, Proteus BioSciences). After three washing cycles in PBS, the samples were probed

with the corresponding Alexa Fluor-conjugated secondary antibodies (Abcam, 1:300) for 2 h at room temperature. Finally, the stained tissues were counterstained with DAPI and mounted on glass slides for confocal microscopy imaging.

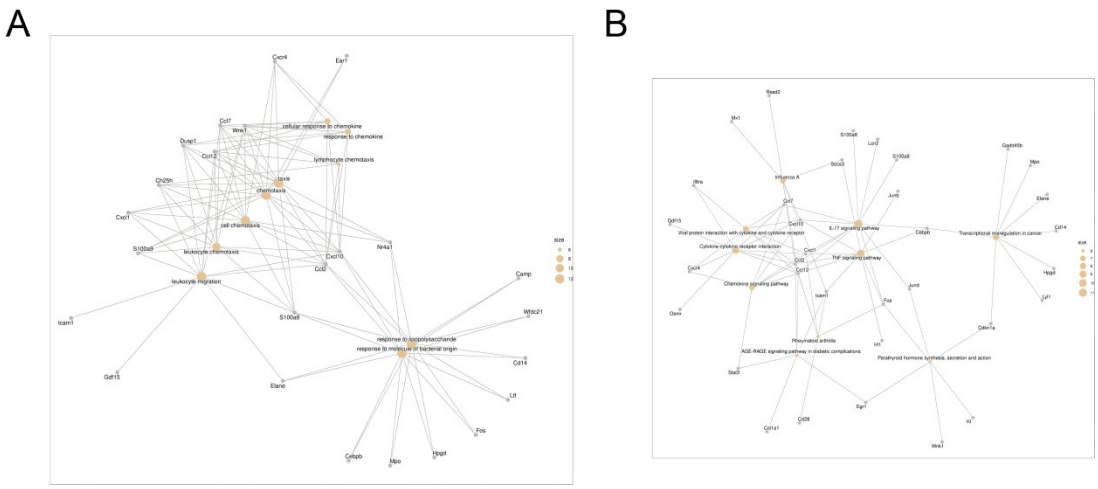

Figure S1. Network visualization of gene-term interactions revealing the immune-dominated landscape of noise-induced hearing loss.

(A) Gene-Concept Network (cnetplot) of the top enriched Gene Ontology (GO) Biological Processes.

(B) Gene-Concept Network of the top enriched Kyoto Encyclopedia of Genes and Genomes (KEGG) pathways.

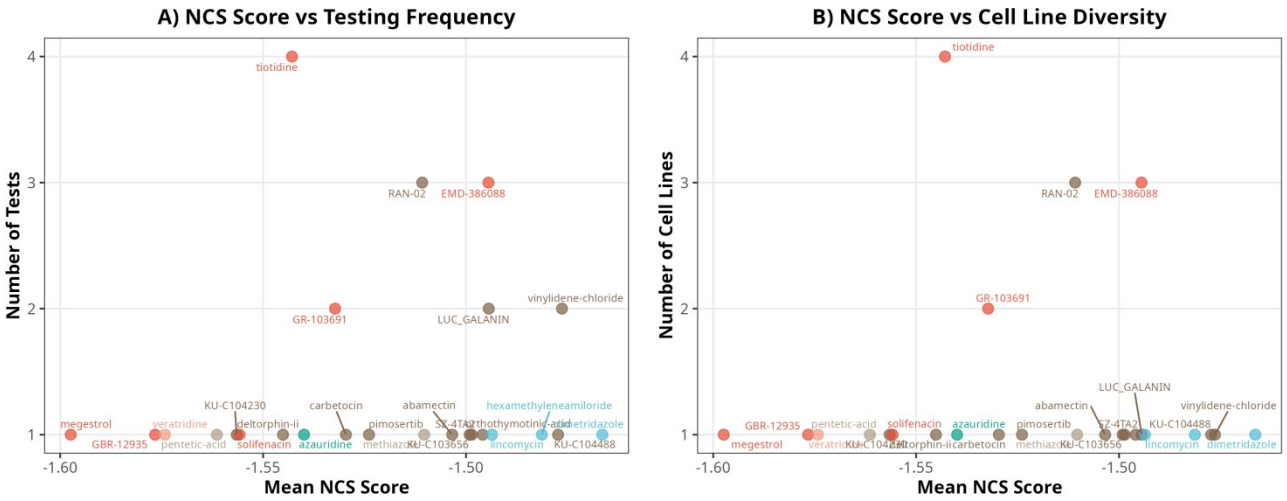

Figure S2. Multiparameter scatter plot analysis of drug candidates based on CMap data. This figure presents a multi-dimensional evaluation of drug candidates by exploring the relationships between Normalized Connectivity Score (NCS), testing frequency, and cell line diversity. The data points are colored according to their Mechanisms of Action (MOA), and the top 25 candidates are labeled using ggrepel for clarity. (A) Scatter plot of NCS versus testing frequency. Drugs tested more frequently (>10 instances) generally do not show the most optimal NCS, suggesting that compounds heavily represented in high-throughput screens may have average matching degrees with our NIHL-specific signature. (B) Scatter plot of NCS versus cell line diversity (number of cell lines tested). A few drugs (e.g., tiotidine) demonstrate consistent efficacy across four different cell lines, indicating potential broad-spectrum therapeutic effects.

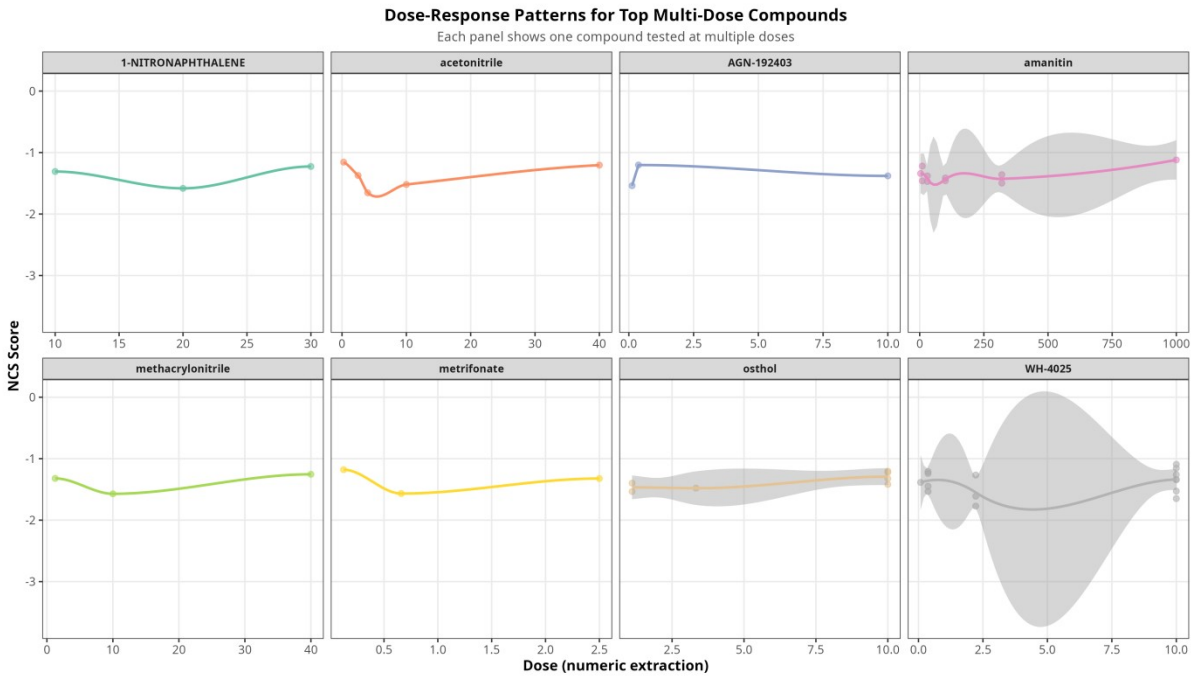

Figure S3. Dose-response analysis of representative drug candidates based on CMap connectivity scores. This facet plot illustrates the dose-dependent profiles of Normalized Connectivity Scores (NCS) for eight selected representative drugs tested across multiple concentrations. The x-axis represents the drug concentration on a logarithmic scale, while the y-axis displays the NCS. Individual data points correspond to distinct perturbational instances available in the CMap database. The solid blue curves indicate LOESS local regression fits, with the surrounding grey shaded areas representing the 95% confidence interval (CI). Diverse patterns, such as monotonic decreasing trends (indicating stronger reversal at higher doses), inverted U-shapes (suggesting optimal intermediate doses), or plateau effects, are observed across different drugs. These profiles provide critical guidance for determining optimal dosing windows for subsequent in vitro and in vivo validation studies.

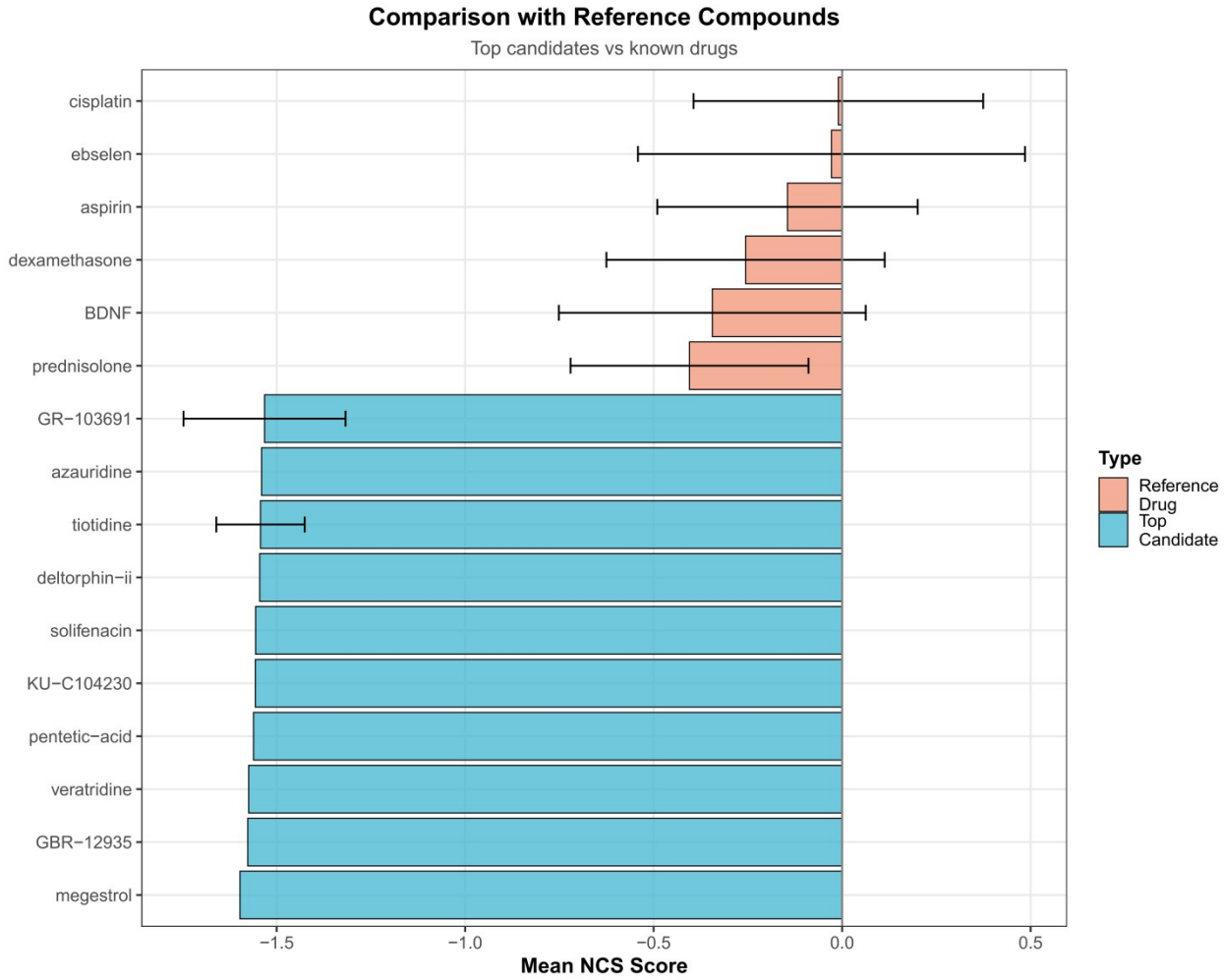

Figure S4. Benchmarking of Top Drug Candidates Against Reference Compounds. This bar chart compares the mean Normalized Connectivity Scores (NCS) of the top 10 candidates identified by our computational screening pipeline (blue bars) with established reference compounds previously reported for auditory protection (orange bars). Error bars represent the standard deviation (SD) of the NCS across multiple perturbational instances in the CMap database. The alignment of our screening results with known otoprotectants serves to validate the predictive power of the signature reversion strategy. High positive scores indicate a strong potential to reverse the NIHL-associated gene expression profile.

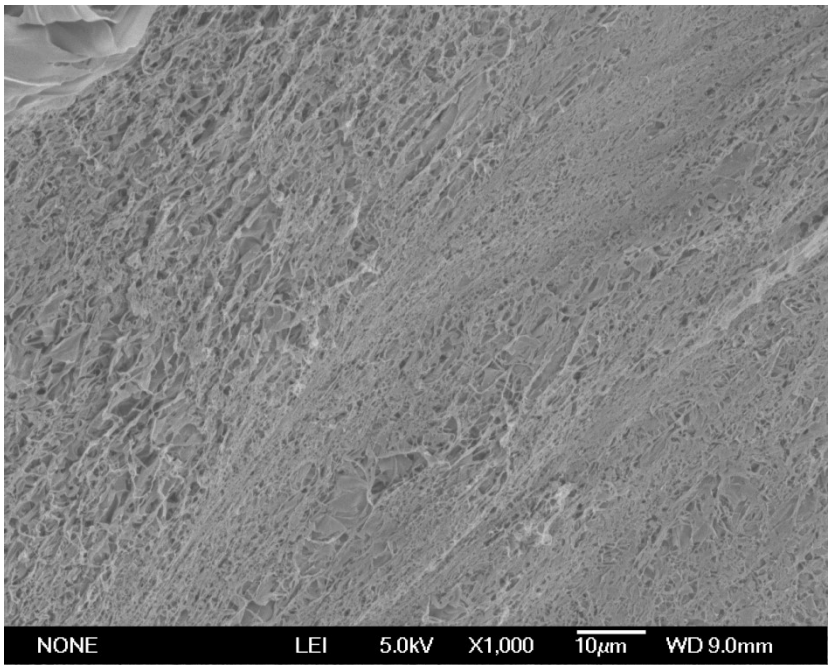

Figure S5. Scanning electron microscopy (SEM) image of chitosan. The micrograph reveals the surface topography of the neat chitosan material. At this magnification, the structure appears relatively dense and irregular, characterized by a rough surface texture without a discernible uniform porous network. Scale bar = 10 μm.

Figure S6. Injectability and self-healing properties of the OKGM/CS hydrogel. Photographs demonstrating the injectability of the hydrogel formulation. The pre-gel solution was loaded into a syringe and extruded through a needle. The extruded material rapidly reformed into a cohesive gel structure, indicating its ability to withstand shear forces during injection and subsequently self-heal. This characteristic is crucial for minimally invasive delivery applications.

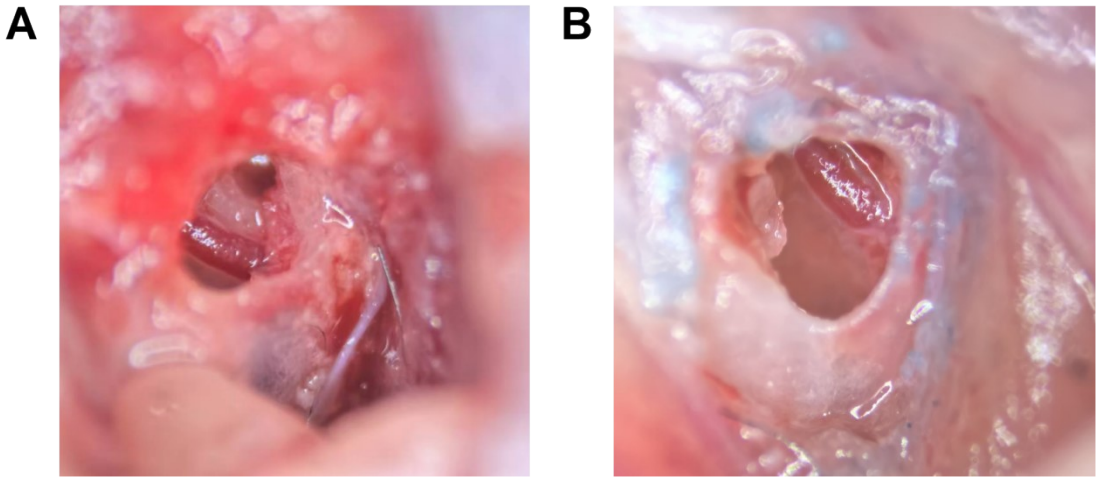

Figure S7. Surgical approach and in vivo safety assessment in the mouse middle ear.

(A) Representative intraoperative stereomicroscope photograph of the auditory bulla fenestration. A small opening was carefully drilled into the lateral wall of the bulla to expose the middle ear cavity. Key anatomical landmarks, including the stapedial artery and the round window niche (RWN), are clearly visible, ensuring precise placement of the hydrogel onto the round window membrane. (B) Macroscopic observation of the middle ear at 10 days post-administration.The cavity is clear with no purulent secretion or inflammatory effusion. The middle ear mucosa appears healthy and non-congested, demonstrating the high in vivobiocompatibility of the OKGM/CS hydrogel during the degradation process.

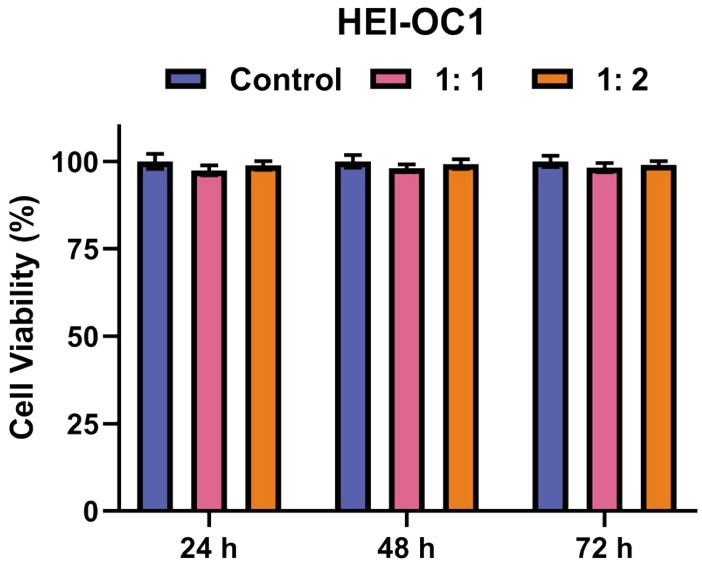

Figure S8. Cell viability of BEAS-2B human epithelial cells (left) and L929 fibroblasts (right) cultured with extracts of 1:1 and 1:2 hydrogels for 24, 48, and 72 h, assessed by CCK-8 assay. Data are presented as mean ± SD (n = 5). No significant difference was observed compared to the control group.

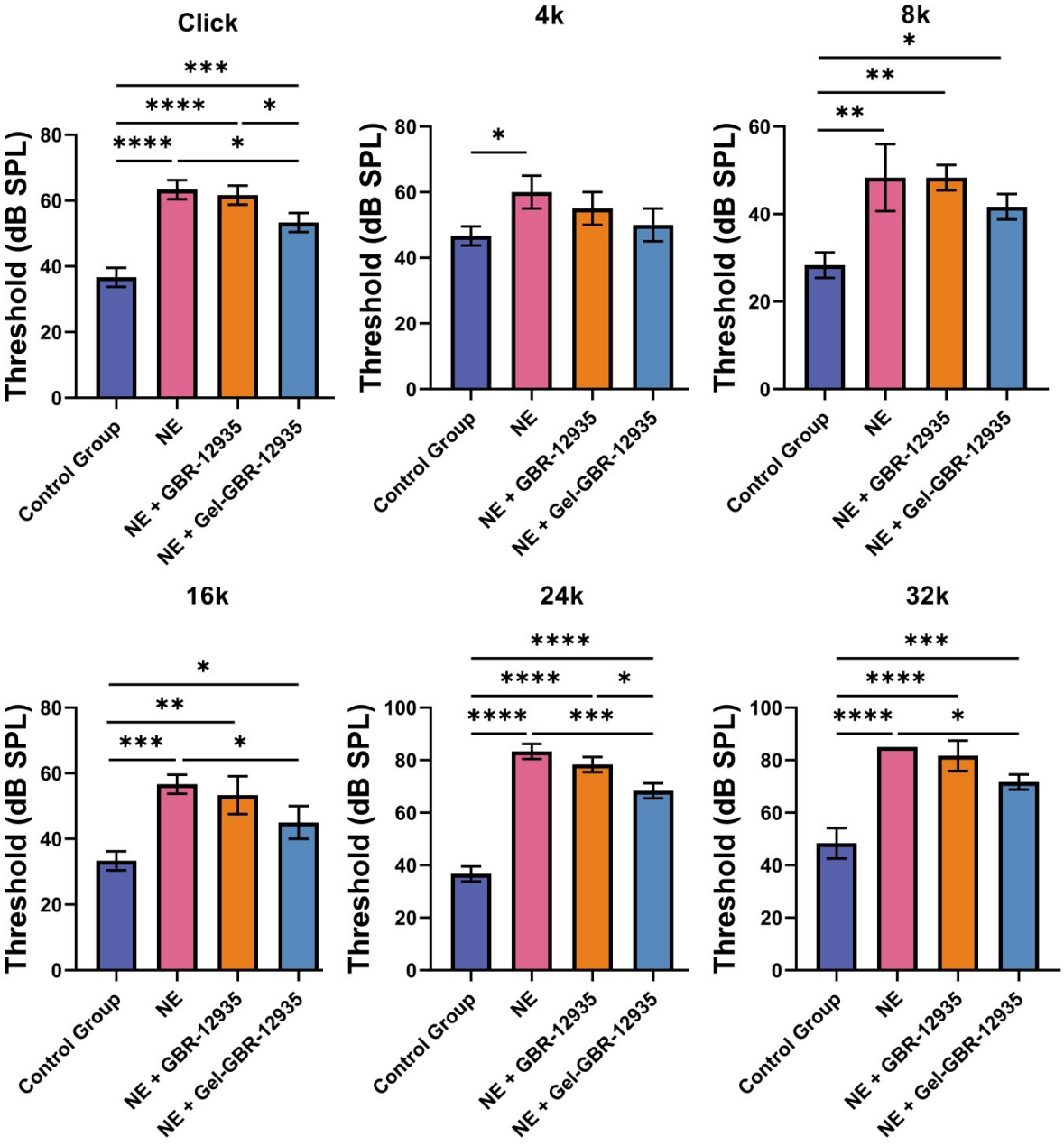

Figure S9. Frequency-specific ABR threshold shifts at day 7 post-noise exposure. Bar graphs illustrating the persistent shift in Auditory Brainstem Response (ABR) thresholds measured at4, 8, 16, 24, and 32 kHz, seven days following noise exposure. Experimental groups include: Control (no noise exposure), Noise (noise + vehicle), Free Drug (noise + aqueous GBR-12935 injection), and Hydrogel (noise + GBR-12935-loaded hydrogel injection). The Noise group exhibited severe, permanent threshold shifts across all tested frequencies. Treatment with GBR-12935 attenuated these shifts, with the Hydrogel group demonstrating significantly superior auditory protection compared to the Free Drug group, particularly at higher frequencies (16-32 kHz), suggesting sustained drug delivery enhances therapeutic efficacy. Data are presented as mean ± SD (n = 3 per group). Statistical significance

was determined by one-way ANOVA with Tukey's post hoc test; asterisks indicate significant differences between groups (*p < 0.05, **p < 0.01, ***p < 0.001, ****p < 0.0001).

Table S1. Summary of Statistical Parameters for Quantitative Analyses

Experiment / Figure	Statistical Test	Factor	F-value (DFn,DFd)	P-value
Ribbon Count (Fig. 7B)	One-way ANOVA	Treatment	F(3,20)=52.36	P<0.0001
Puncta Area (Fig. 7C)	One-way ANOVA	Treatment	F(3,116)=47.10	P<0.0001
ABR Thresholds (Fig. 7D)	Two-way ANOVA	Treatment	F(3,48)=174.5	P<0.0001